Electronic Supplementary Material (ESI) for Chemical Communications.
This journal is © The Royal Society of Chemistry 2017

Supporting Information for

Two-State Reactivity in C-H Activation by a Four-Coordinate Iron(0) Complex

Anne K. Hickey, Sean Lutz, Chun-Hsing Chen and Jeremy M. Smith

Indiana University Department of Chemistry
800 E. Kirkwood Ave., Bloomington, IN 47405
Corresponding author email address: smith962@indiana.edu

Experimental

General Considerations. All manipulations were performed under a nitrogen atmosphere by standard Schlenk techniques or in a glove box. Glassware was dried at 130 °C overnight before cooling under a dynamic vacuum in an antechamber. Diethyl ether (Et_2O), tetrahydrofuran (THF), toluene, and pentane were purified by a Glass Contour solvent purification system. Celite was dried overnight at 130 °C under vacuum. The complexes $Ph_2B(^tBuIm)_2Fe(CO)_3$[1] and $\{K(Ph_2B(^tBuIm)_2Fe(CO)_2)\}_2(THF)_4$[1] were prepared by literature methods. Encapsulating agent 2.2.2-crytand was purchased from TCI America and used as received. ^1H NMR spectroscopic data were recorded on a Varian spectrometers. Solution magnetic susceptibilities were determined by Evans' method.[2] IR spectra were recorded with a Perkin Elmer spectrophotometer, with a Specac Variable Temperature Cell Controller and Specac Variable Temperature Cell for variable-temperature experiments. UV-Vis spectroscopic data were collected on an Agilent Technologies Cary 60 UV-Vis instrument, with a Unisoku Scientific Instruments cryostat for variable-temperature experiments. Elemental analysis was conducted by Midwest Microlab, LLC (Indianapolis, IN).

[K(2.2.2-cryptand)][$Ph_2B(^tBuIm)_2Fe(CO)_2$] (1/2). A vial was charged with $Ph_2B(^tBuIm)_2Fe(CO)_3$ (75 mg, 0.14 mmol), KC_8 (19 mg, 0.14 mmol), and 10 mL THF. The slurry was stirred for 2 h, and 2.2.2-cryptand (51 mg, 0.15 mmol) was added as a solid, turning the slurry from purple to green. After stirring for 2 h, the slurry was filtered through Celite and taken to dryness, giving [K(2.2.2-cryptand)][$Ph_2B(^tBuIm)_2Fe(CO)_2$] as a green powder (126 mg, 98% yield). Crystals suitable for X-ray diffraction were grown from a concentrated THF solution layered with pentane, stored at -35 °C for 2 days. ν_{CO}: 1930, 1859, 1846, 1753 cm^{-1} (KBr pellet), 1926, 1860, 1845, 1758 cm^{-1} (THF). Analysis Cald. for $C_{46}H_{68}BFeKN_6O_8$: C 58.85, H 7.30, N 8.95; Found: C 58.39, H 7.53, N 8.89.

Supplementary Figures

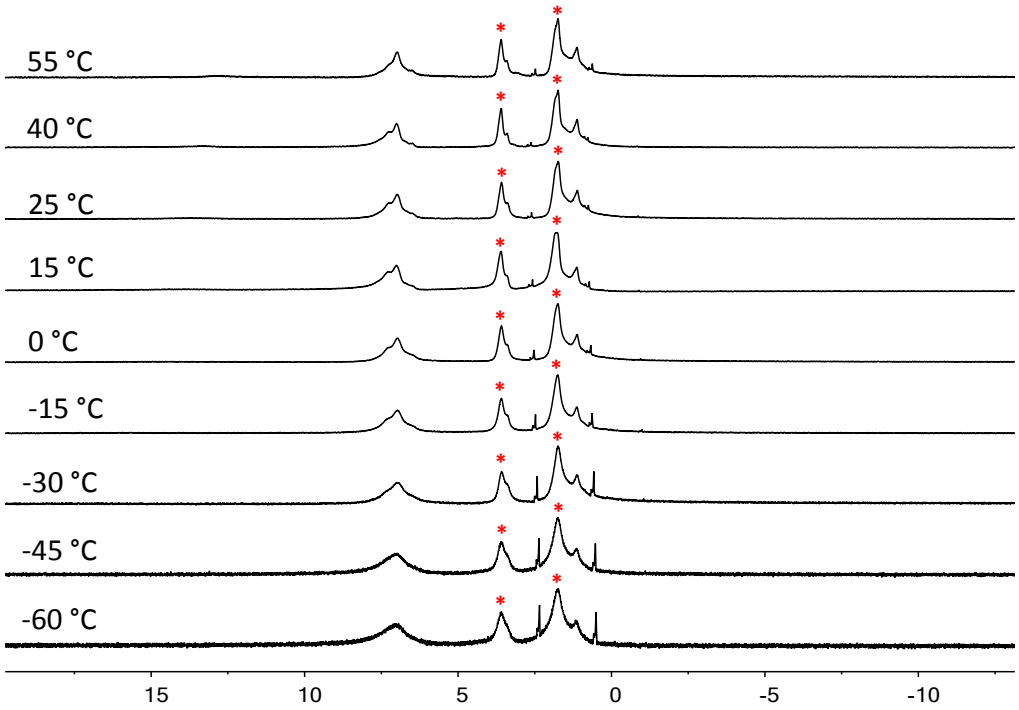

Figure S1. VT NMR spectra (500 MHz, THF-d_8 (*)) of [K(2.2.2-cryptand)] [$Ph_2B(^tBuIm)_2Fe(CO)_2$] (**1/2**).

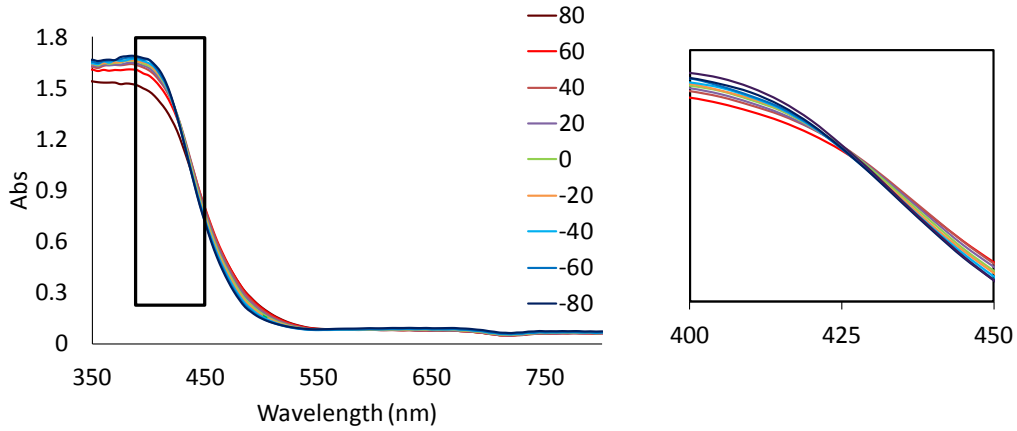

Figure S2. Variable-temperature UV-Vis spectra of [K(2.2.2-cryptand)][$Ph_2B(^tBuIm)_2Fe(CO)_2$] (**1/2**) in THF, between 80 and -80 °C in increments of 20 °C. An isosbestic point is observed at 425 nm.

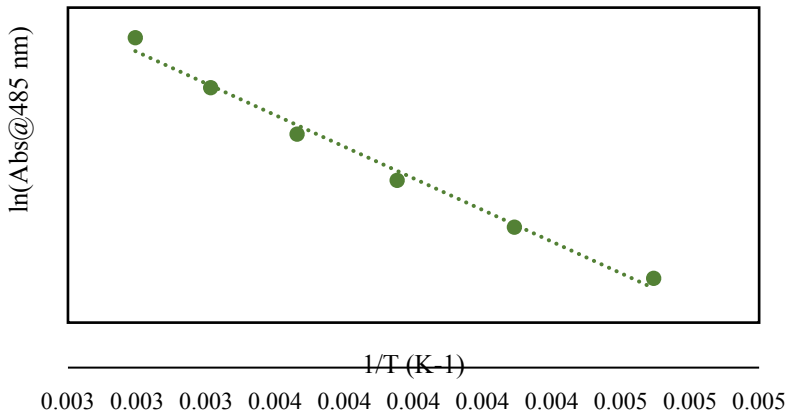

Figure S3. Van't Hoff plot of [K(2.2.2-cryptand)][$Ph_2B(^tBuIm)_2Fe(CO)_2$] (**1/2**) ln(Abs) versus 1/T. Thermodynamic formation parameters extracted from the linear fit are ΔH^o = 0.34(2) kcal mol^{-1}, and ΔS^o = -0.0014(1) Kcal mol^{-1} K^{-1} for the decay of **1**. At 150 K, ΔG = 0.55(2) Kcal mol^{-1}, giving K_{eq} = 6.32. At 298 K, ΔG^o = 0.76(2), giving K_{eq} = 3.61.

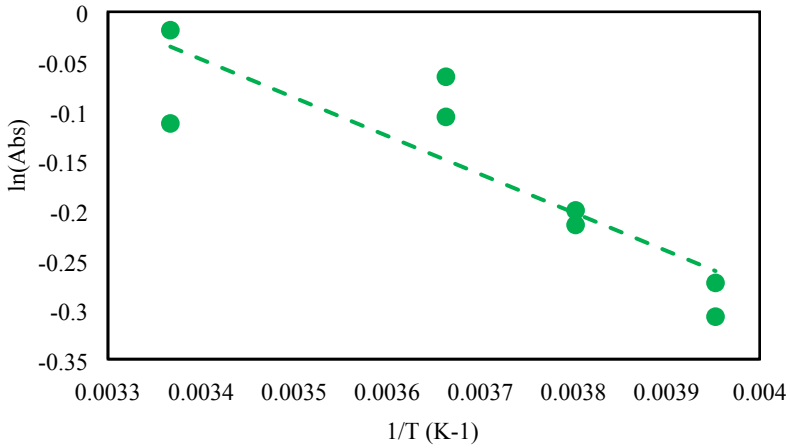

Figure S4. Van't Hoff plot of [K(2.2.2-cryptand)][$Ph_2B(^tBuIm)_2Fe(CO)_2$] (**1/2**) showing ln(Abs) versus 1/T showing the decay of **1** as temperature is decreased from 24 °C to -20 °C. Both C-O stretches are shown. Thermodynamic formation parameters extracted from the linear fit are ΔH^o = 0.76(18) Kcal mol^{-1} and ΔS^o = 0.003(1) Kcal $mol^{-1}K^{-1}$. The ΔG^o values at 298 and 150 K are 0.018(6) and 0.39(13) kcal mol^{-1}, respectively. The values for K_{eq} at 298 and 150 K are 0.96 and 0.27, respectively.

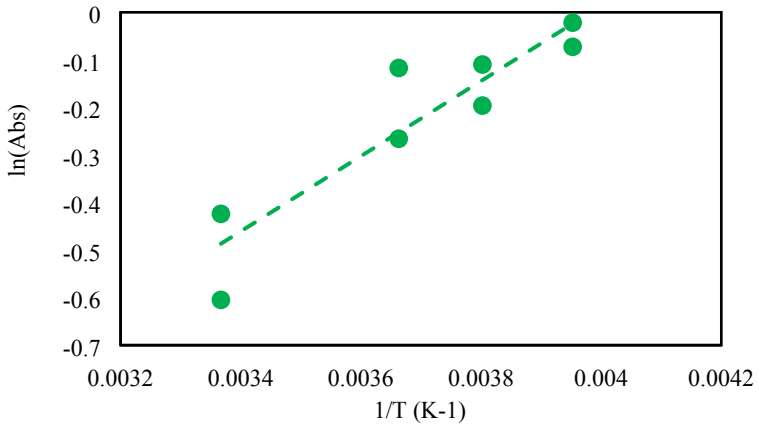

Figure S5. Van't Hoff plot of [K(2.2.2-cryptand)][$Ph_2B(^tBuIm)_2Fe(CO)_2$] (**1/2**) showing ln(Abs) versus 1/T showing the formation of **2** as temperature is decreased from 24 °C to -20 °C. Both C-O stretches are shown. Thermodynamic formation parameters extracted from the linear fit are ΔH^o = -1.57(27) Kcal mol^{-1} and ΔS^o = -0.006(1) Kcal $mol^{-1}K^{-1}$. The ΔG^o values at 298 and 150 K are 0.29(7) and -0.63(15) kcal mol^{-1}, respectively. The values for K_{eq} at 298 and 150 K are 0.88 and 1.66, respectively.

Computational Details

All calculations were performed using density functional theory as implemented in the Orca computational software package.[3] Geometry optimizations for all complexes were performed with the M06 functional and Dunning style cc-pVDZ basis sets. The electronic energies (single point energy corrections) were reevaluated with cc-pVTZ basis set that includes a double set of polarization functions for a more accurate overall electronic energy. Additionally, the Fe center was treated with the LANL(TZ) Los Alamos effective core potential to increase computational efficiency. Vibrational/rotational/translational entropies of the solute(s) were included using standard thermodynamic approximations. Solvation energies were determined by a self-consistent reaction field (SCRF) approach. Solvation calculations were carried out on optimized gas phase geometries employing the dielectric constant of $\varepsilon = 7.34$ (THF). The standard set of optimized radii was used to generate the solute surface. All structures were verified to be minima on the potential energy surface by the removal of imaginary frequencies. Transition states were verified by the inclusion of one imaginary mode. Determination of the change in solution phase free energy $\Delta G_{(sol)}$ was calculated as follows:

$$\Delta G_{(sol)} = \Delta G_{(gas)} + \Delta\Delta G_{solv}$$

$$\Delta G_{(gas)} = \Delta H_{(gas)} - T\Delta S_{(gas)}$$

$$\Delta H_{(gas)} = \Delta E_{(scf)} + \Delta ZPE$$

$\Delta G_{(gas)}$ = change in gas phase free energy; $\Delta\Delta G_{solv}$ = change in free energy pf solvation; $\Delta H_{(gas)}$ = change in gas phase enthalpy; T = temperature (298.15 K); $\Delta S_{(gas)}$ = change in gas phase entropy; $\Delta E_{(scf)}$ = self-consistent field energy or the electronic energy at the triple-ζ level; ΔZPE = change in vibrational zero point energy.

Since DFT functionals have major deficits in dealing with energy differences in spin states, a set of 6 different functionals that vary in the degree of Hartree-Fock exchange were used to assess the difference in spin state energies. This allows the DFT calculations to be parameterized according to experimental results through the choice of functional.

Two spin states were considered for the $Ph_2B(^tBuIm)_2Fe(CO)_2$ (**1**), namely singlet ($S = 0$) and triplet ($S = 1$). Hybrid and meta-hybrid functionals that include HF exchange show the largest triplet singlet gap. This is not surprising considering HF exchange overstabilize systems high spin states due to favorable spin exchange.[4] Local functionals show a smaller gap with PBE having the smallest (Table S1). Three spin states were considered for the product, $Ph_2B(^tBuIm)(CH_2C(CH_3)_2Im)Fe(CO)_2H$ (**2**): $S = 0$, 1 and 2. In this case, only the singlet converged to a structure consistent with that observed by X-ray crystallography. Unsurprisingly, given the strong field ligand environment in **2**, all attempts to converge the higher spin states were unsuccessful.

Table S1. Relative free energies of **1** in THF solution ($\Delta G_{(sol)}$ kcal/mol)

	M06	M06-L	BLYP	B3LYP	PBE	ωB97
$S = 0$	14.07	12.96	11.82	21.03	8.23	13.16
$S = 1$	0.00	0.00	0.00	0.00	0.00	0.00

The thermodynamics of the C-H activation reaction were also found to be heavily dependent on the choice of functional, with PBE providing a free energy that is most consistent with that determined experimentally (Table S2). All further calculations were therefore conducted using the PBE functional and cc-pVTZ basis set (perhaps give functional/ basis set). These calculations give structures in good agreement with those determined crystallographically (Table S3).

Table S2. Functional dependence of the free energies for the conversion of **1** to **2**.

	M06	M06-L	BLYP	B3LYP	PBE	ωB97
$\Delta G_{(sol)}$	14.61	8.68	9.34	12.96	1.26	9.88

Table S3. Comparison of selected metrical parameters from the single X-ray crystal structures and DFT calculations.

***S* = 1 Reactant**	**Calculated**	**Experimental**	**Calculated**	**Experimental**
Fe-C_{im}[a]	2.073	1.953		
Fe-C_{im}	2.078	2.035		
Fe-CO			1995	1930
Fe-CO			1922	1859
***S* = 0 Product**				
Fe-C_{im}*	2.053	2.035		
Fe-C_{im}	1.918	1.953		
Fe-C	2.090	2.167		
Fe-CO			2063	1846
Fe-CO			2014	1753

[a] Due to the crystallographic disorder, the experimental Fe-C bond length is significantly shorter than for the optimized structure.

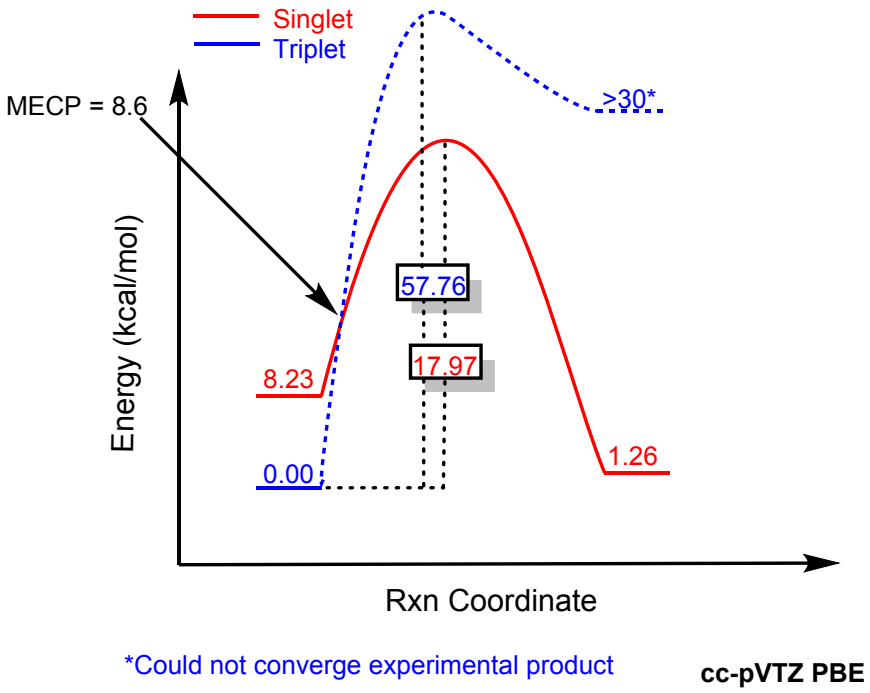

Figure S6. Reaction coordinate for the conversion of $Ph_2B(^tBuIm)_2Fe(CO)_2$ (**1**) to $Ph_2B(^tBuIm)(CH_2C(CH_3)_2Im)Fe(CO)_2H$ (**2**) in THF solvent (PBE/cc-pVTZ). Relative free energies are shown in kcal/mol.

A reaction coordinate diagram was constructed using the relative free and transition state energies (Figure S6). The reaction surface for the conversion of $Ph_2B(^tBuIm)_2Fe(CO)_2$ (**1**) to $Ph_2B(^tBuIm)(CH_2C(CH_3)_2Im)Fe(CO)_2H$ (**2**) in THF shows three thermally accessible species. For the reactant (**1**), a triplet ($S = 1$) is tetrahedral is favored over the square planar reaction 8.2 kcal/mol with the PBE functional. The triplet (S = 1) product (**2**) could not be converged to a structure that is consistent with that determined by X-ray crystallography. In order to get an estimate of the energy difference between the singlet and triplet spin states, a single point energy calculation was performed for the singlet product structure (**2**) with a triplet spin state. This single point energy calculation revealed an electronic energy difference of over 30 kcal/mol. Additionally, TD-DFT calculations on the singlet product (**2**) show that the first excited state is 77.51 kcal/mol higher in energy than the ground state.

Transition state calculations reveal the only thermally accessible spin surface is the singlet, with $\Delta G^{\ddagger} = 18.0$ kcal/mol. Analysis of the molecular orbitals at the transition state shows why the triplet is so much higher in energy than the singlet surface. The triplet SOMO is a Fe based σ*

orbital that is antibonding with respect to all bonds (Figure S7), while the singlet HOMO shows weakening of the C-H bond concomitant with Fe-C and Fe-H bond formation, i.e. C-H oxidative addition.

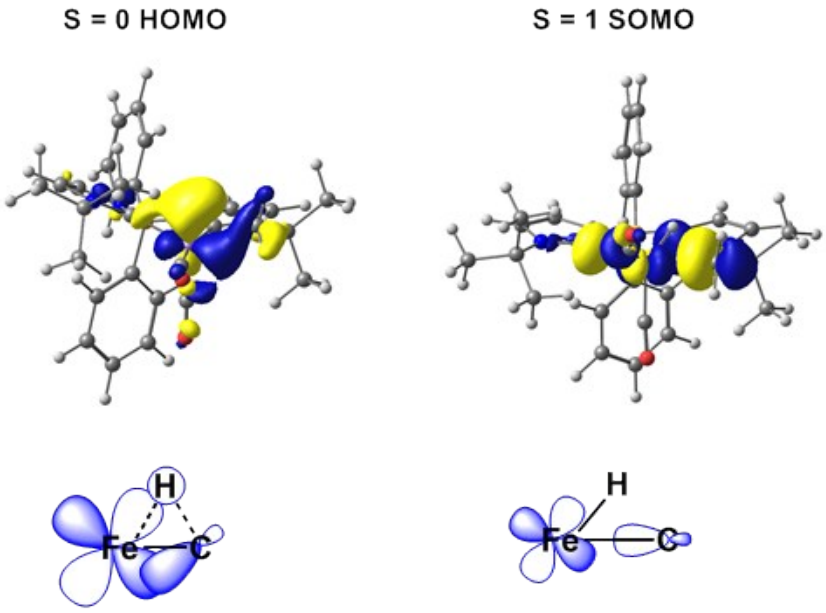

Figure S7. Frontier molecular orbitals for the HOMO of the singlet and the SOMO of the triplet. The triplet SOMO reveals largely antibonding character with population of a σ* orbital driving the energy of the TS higher.

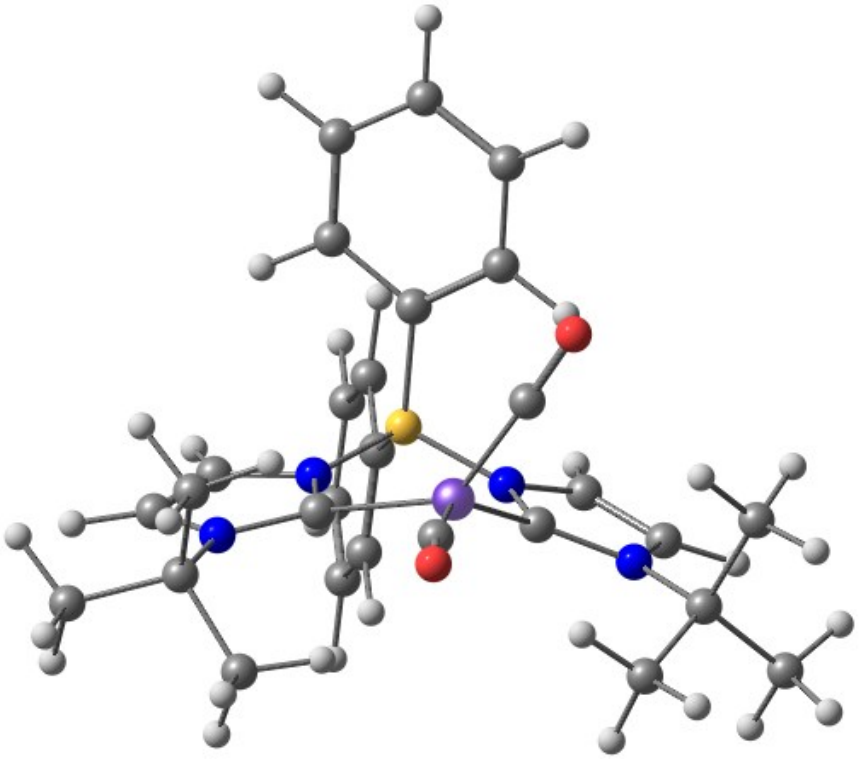

Figure S8. Geometry of the MECP. The MECP structure ($\tau_4 = 0.57$) is intermediate between the singlet ($\tau_4 = 0.19$) and triplet ($\tau_4 = 0.92$) reactant structures.

Since the C-H activation reaction involves an intersystem crossing, a minimum energy crossing point (MECP) was located using the algorithm by developed Harvey[5] as implemented in the Orca software package. The geometry of the MECP (Figure S8) shows rotation of the OC-Fe-CO ligand plane with respect to the bis(carbene)borate ligand, creating a structure that is intermediate between the singlet and triplet geometries.

Crystallographic Information

Data collection

The data collection was carried out using Mo Kα radiation (graphite monochromator) with a selected frame time and detector distance. A randomly oriented region of reciprocal space was surveyed to achieve complete data with a redundancy of 4. Sections of frames were collected with 0.50º steps in ω and ϕ scans. Data to a resolution of 0.86 Å were considered in the reduction. Final cell constants were calculated from the xyz centroids of strong reflections from the actual data collection after integration (SAINT).[6] The intensity data were corrected for absorption (SADABS).[7]

Structure solution and refinement

The space groups were determined based on intensity statistics and systematic absences. The structure was solved using SIR-92[8] and refined (full-matrix-least squares) using the Oxford University Crystals for Windows system.[9] A direct-methods or intrinsic methods solution was calculated, which provided most non-hydrogen atoms from the E-map. Full-matrix least squares/difference Fourier cycles were performed, which located the remaining non-hydrogen atoms. All non-hydrogen atoms were refined with anisotropic displacement parameters. The hydrogen atoms were placed in ideal positions and refined as riding atoms.

[K(2.2.2-cryptand)][$Ph_2B(^tBuIm)_2Fe(CO)_2$] (Complex 1/2)

Empirical formula	C54 H84 B Fe K N6 O10	
Formula weight	1083.03	
Crystal color, shape, size	green-blue block, 0.32 × 0.15 × 0.12 mm^3	
Temperature	150(2) K	
Wavelength	0.71073 Å	
Crystal system, space group	Monoclinic, $P2_1/n$	
Unit cell dimensions	a = 12.8202(4) Å	α = 90°.
	b = 14.9253(4) Å	β = 95.4151(15)°.
	c = 30.2522(8) Å	γ = 90°.
Volume	5762.8(3) $Å^3$	
Z	4	
Density (calculated)	1.248 Mg/m^3	
Absorption coefficient	0.393 mm^{-1}	
F(000)	2320	

Data collection

Diffractometer	APEX II Kappa Duo, Bruker
Theta range for data collection	1.35 to 27.55°.
Index ranges	-16<=h<=16, -17<=k<=19, -37<=l<=39
Reflections collected	49153
Independent reflections	13204 [R(int) = 0.0398]
Observed Reflections	9046
Completeness to theta = 27.55°	99.1 %

Solution and Refinement

Absorption correction	Semi-empirical from equivalents
Max. and min. transmission	0.9543 and 0.8845
Solution	Intrinsic methods
Refinement method	Full-matrix least-squares on F^2
Weighting scheme	$w = [\sigma^2Fo^2 + AP^2 + BP]^{-1}$, with
	$P = (Fo^2 + 2\,Fc^2)/3$, A = 0.0728, B = 5.0780
Data / restraints / parameters	13204 / 187 / 699
Goodness-of-fit on F^2	1.052
Final R indices [I>2sigma(I)]	R1 = 0.0603, wR2 = 0.1481
R indices (all data)	R1 = 0.0953, wR2 = 0.1654
Largest diff. peak and hole	1.336 and -1.036 $e.Å^{-3}$

References

1. Hickey, Anne K.; Lee, Wei-Tsung; Chen, Chun-Hsing; Pink, Maren; Smith, Jeremy M. *Organometallics* **2016**, *35*, 3069-3073.
2. Baker, M.V.; Field, L.D.; Hambley, T.W. *Inorg. Chem*. **1988**, 27, 2872.
3. F. Neese, *WIREs Comput. Mol. Sci.* 2012, **2**, 73.

4. H. Paulsen, L. Duelund, H. Winkler, H. Toftlund, A.X. Trautwein, *Inorg. Chem.* 2001, **40**, 2201.

5. J.N. Harvey, M. Aschi, H. Schwarz, W Koch, *Theor. Chem. Acc* 1998, **99**, 95

6. SAINT, Bruker Analytical X-Ray Systems, Madison, WI, current version.
7. An empirical correction for absorption anisotropy, R. Blessing, *Acta Cryst*. **1995**, *A51*, 33-38.
8. Altomare, A; Cascarano, G; Giacovazzo, G.; Guagliardi, A.; Burla, M. C.; Polidori, G.; Camalli, M. *J. Appl. Cryst.* **1994**, *27*, 435.
9. Betteridge, P. W.; Carruthers, J. R.; Cooper, R. I.; Prout, K.; Watkin, D. J. *J. Appl. Cryst*. **2003**, *36*, 1487.